# Double-atomic-layer Tl-Mg compound on a Si(111) surface with advanced electronic properties

A. Y. Tupchaya,[1] L. V. Bondarenko,[1] Y. E. Vekovshinin,[1,2] A. A. Yakovlev,[1] A. N. Mihalyuk,[1,2] D. V. Gruznev,[1,*] C. R. Hsing,[3] C. M. Wei,[3] A. V. Zotov,[1] and A. A. Saranin[1]

[1]*Institute of Automation and Control Processes FEB RAS, 5 Radio Street, 690041 Vladivostok, Russia*

[2]*School of Natural Sciences, Far Eastern Federal University, 690950 Vladivostok, Russia*

[3]*Institute of Atomic and Molecular Sciences, Academia Sinica, P.O. Box 23-166, Taipei 11529, Taiwan*

(Received 26 April 2020; revised manuscript received 11 June 2020; accepted 15 June 2020; published 26 June 2020)

We report on the formation and comprehensive study of atomic and electronic structures of a new Tl-Mg two-dimensional compound reconstruction with $\sqrt{3} \times \sqrt{3}$ periodicity on a Si(111) substrate. Owing to properties of its constituent elements and crystal structure with a breathing kagome lattice of Mg and a dense Tl layer (4/3 monolayer), this double-layer system displays promising features, including spin-split metallic bands, nearly flat bands, and a saddle point with corresponding divergences in the local density of states. These features indicate the possibility that strongly correlated electronic states exist in this structure after tuning the Fermi level position. In accordance with the $C_3$ symmetry, we observe spin-orbit-coupling-driven Rashba-type spin splitting with spin degeneracy at the $\bar{M}$ point and Zeeman-like splitting at the $\bar{K}$ point. In contrast to the previously reported cases, splitting at the $\bar{K}$ point is significant to produce fully out-of-plane spin-polarized cones. Due to opposite Berry curvatures at the $\bar{K}$ and $\bar{K}'$ points of the hexagonal surface Brillouin zone, spins at these valleys have opposite signs, which ensure effective spin-pseudospin coupling.

DOI: 10.1103/PhysRevB.101.235444

## I. INTRODUCTION

Metal-induced surface reconstructions on semiconductors have attracted considerable attention as promising two-dimensional (2D) materials. Among them, heavy-metal-based reconstructions display a rich variety of intriguing properties making them useful for prospective applications, including 2D superconductivity (including topological superconductivity) [1–4], Rashba-type spin-splitting of surface states [5–10], and quantum spin Hall insulators [11,12]. Being the heaviest stable element in group III, thallium (Tl) contributes to the strong spin-orbit coupling (SOC) in surface structures inducing a number of interesting phenomena. A pseudomorphic Tl monolayer (1 × 1 Tl reconstruction) with abrupt spin rotation [13–16] has fully spin-polarized valleys in the surface Brillouin zone (SBZ) that suppresses the backscattering of spin charge after low Tl doping [17]. A double-layer Tl structure [18,19] undergoes a superconducting transition at 0.96 K and superconductor-insulator transition under a magnetic field with an intermediate Bose metal state [20]. These features make the Tl/Si(111) layers promising for constructing semiconductor spintronic devises and exploring spin transport phenomena.

Despite the presence of 2D Tl structures on other surfaces [21], the number of such materials is limited and the natural expansion of this base of knowledge is to use binary alloys and Tl-based 2D compounds. Indeed, such compound reconstructions on Si(111) and Ge(111) substrates [22–25] often demonstrate advanced properties associated with the spin-splitting of surface-state bands due to the Rashba effect. For example, the (Tl, Pb)/Si(111) system transforms into the superconducting state at 2.25 K, followed by the Berezinskii-Kosterlitz-Thouless mechanism [22], and the (Tl, Au)/Si(111) system with $\sqrt{7} \times \sqrt{7}$ periodicity demonstrates the weak antilocalization effect at the atomic-scale limit [25].

In the present paper, we report on the formation and comprehensive study of atomic and electronic structures of another Tl-based 2D compound, a Tl-Mg binary surface reconstruction with $\sqrt{3} \times \sqrt{3}$ periodicity on Si(111). Owing to properties of its constituent elements [strong SOC of Tl and good reducing ability of magnesium (Mg)], this double-layer structure with in-plane asymmetry displays promising features, such as nearly flat bands and a saddle point with corresponding divergences in the local density of states (LDOS) spectra, spin-split metallic bands, and spin-pseudospin coupling in out-of-plane polarized valleys at the corners of the SBZ. Since 2D materials in general are considered to be an essential part of semiconductor spintronics [26], the aforementioned properties of the Tl-Mg 2D compound make it a suitable candidate for studies of physical properties such as spin transport phenomena and the spin valley locking effect and possibly for optoelectronic studies with circularly polarized light.

## II. EXPERIMENTAL AND CALCULATION DETAILS

Experiments were performed in an ultrahigh-vacuum Omicron MULTIPROBE system (base pressure, $\leqslant 2.0 \times 10^{-10}$ Torr) by means of scanning tunneling microscopy (STM), low-energy electron diffraction (LEED), and angle-resolved photoelectron spectroscopy (ARPES). Si(111) samples were

*gruznev@iacp.dvo.ru

 

first outgassed at 600 °C for several hours and then cleaned *in situ* by direct-current annealing at 1280 °C. Thallium and magnesium were deposited from heated tantalum tubes. Deposition rates were calibrated using STM observation of the Si(111) $1 \times 1$ Tl [saturation coverage, 1 ML (monolayer)] and Si(111) $3 \times 1$ Mg (1/3 ML) surface reconstructions, respectively. STM images were acquired using an Omicron variable-temperature STM-XA operating in constant-current mode. Mechanically cut PtIr tips were used as STM probes after annealing in vacuum. ARPES measurements were conducted at 78 K using a VG Scienta R3000 electron analyzer and high-flux He discharge lamp ($h\nu = 21.2$ eV) with a toroidal-grating monochromator as a light source.

Calculations were based on density functional theory (DFT) as implemented in the Vienna Ab initio Simulation Package (VASP) [27,28] using a plane-wave basis set. The projector-augmented wave (PAW) approach [29] was used to describe the electron-ion interaction and the generalized gradient approximation (GGA) of Perdew, Burke, and Ernzerhof (PBE) [30] was employed as the exchange-correlation functional. The scalar relativistic effect and the spin-orbit interaction were taken into account. To simulate the Tl-Mg reconstruction we used a slab consisting of four bilayers of silicon at the PBE-optimized bulk lattice constants. Hydrogen atoms were used to passivate the dangling bonds at the bottom of the slab. The atomic positions of adsorbed atoms and atoms of Si layers within the three bilayers of the slab were optimized. Substrate atoms of the deeper layers were kept fixed at the bulk crystalline positions. The kinetic cutoff energy was 250 eV, and a $5 \times 7 \times 1$ $k$-point mesh was used to sample the SBZ. The geometry optimization was performed without considering SOC until the residual force on atoms was lower than 10 meV/Å. For surface band structure calculations we use the slab model and apply the DFT-1/2 self-energy correction method [31,32], which only requires the addition of a self-energy correction potential, calculated from a half-ionized free atom, to the standard DFT potential (PAW-PBE in our case).

## III. RESULTS AND DISCUSSION

The growth condition for the Tl-Mg compound surface reconstructions involves Mg deposition at room temperature (RT) onto the Tl-saturated silicon (111) surface. During the deposition, a mixture of a single-layer $\sqrt{13} \times \sqrt{13}$ structure and a double-layer $\sqrt{3} \times \sqrt{3}$ film simultaneously forms. (The double-layer nature of the film is revealed from the height analysis at early stages of formation.) If the initial Tl coverage is close to 1 ML (Si(111) $1 \times 1$ Tl reconstruction [33]), single- and double-layer structures occupy roughly equal areas (~50/50), implying that they have similar Mg, but different Tl, coverages such that

$$\theta_{\mathrm{Tl}}^{\sqrt{13}} < \theta_{\mathrm{Tl}}^{1\times1} < \theta_{\mathrm{Tl}}^{\sqrt{3}}.$$

To maximize the area of the double-layer $\sqrt{3} \times \sqrt{3}$ film [34], an additional ~0.5 ML of Tl is required, thus we used a mixture of $1 \times 1$ Tl (1 ML) and $6 \times 6$ Tl (2.24 ML [19]) with a total Tl coverage of ~1.5 ML as a starting surface. Once extra Tl is provided, Mg deposition at RT results in the formation

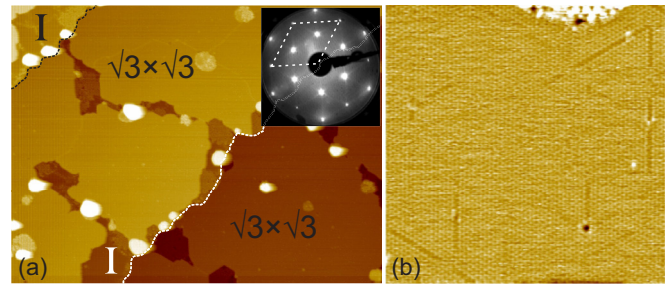


FIG. 1. Growth of the (Tl,Mg)/Si(111) double-layer film. (a) A $400 \times 300$ nm$^2$ STM image of the surface obtained by 1-ML Mg deposition onto the Tl/Si(111) surface ($\theta_{\mathrm{Tl}} \approx 1.5$ ML) at RT. "I" stands for a single-layer $\sqrt{13} \times \sqrt{13}$ (Tl,Mg) structure. Step edges are outlined to guide the eye. Inset: LEED pattern (35 eV) with the $(1 \times 1)$ unit cell outlined. (b) A $40 \times 40$ nm$^2$ STM image of the $\sqrt{3} \times \sqrt{3}$ (Tl,Mg) layer.

of $\sqrt{3} \times \sqrt{3}$ (Tl,Mg) over almost the entire surface, yielding a sharp $\sqrt{3} \times \sqrt{3}$ LEED pattern, as shown in Fig. 1. Remains of the $\sqrt{13} \times \sqrt{13}$ structure are labeled "I" in Fig. 1(a).

The surface of the film has a very small corrugation associated with the $\sqrt{3} \times \sqrt{3}$ lattice, less than 0.1 Å. The lattice is interrupted by fainting lines typically pinned at local defects. The presence of the lines is also manifested in LEED patterns as streaks around the $\sqrt{3}$-order spots. Close to the lines, the honeycomb $\sqrt{3} \times \sqrt{3}$ lattice gradually turns into a hexagonal one with the same periodicity by upthrusting the honeycomb's sublattices (different ones on the opposite sides of a line), thus forming two antiphase domains with the line being the domain boundary as illustrated in Fig. 2(d).

Low-temperature STM measurements (Fig. 3) revealed that this surface in the ground state is hexagonal with one protrusion and one depression per $\sqrt{3} \times \sqrt{3}$ unit cell. Seemingly uniform at RT, the surface breaks down to domains with a drastic increase in the domain wall (DW) density compared to that at RT. For an unclear reason, the domains have a "saw"-like shape confined by a long straight DW at one edge and a zigzag DW at the other one. It can be seen that some short segments of DWs appear noisy due to continuous changing of their positions even at 110 K. Thus, the RT STM appearance of this surface with a honeycomb lattice and fainting DWs can be interpreted as a time-averaged pattern in which one protrusion constantly changes its position between two possible sites in the unit cell. Note that only bright protrusions form domains (they occupy opposite half-unit cells in adjacent domains), while all depressions (including those in the DW area) belong to the same lattice [Fig. 3(c)]. We argue that bright protrusions belong to the second (top) layer of this double-layer structure, and only atoms in the top layer shift their positions at RT in a collective motion rendering the illusive honeycomb lattice.

The atomic arrangement of the $\sqrt{3} \times \sqrt{3}$ (Tl,Mg) surface was elucidated by DFT calculations of various possible configurations taking into account its double-layer structure and experimentally established Tl coverage of ~1.5 ML. A various amount of Mg atoms (from one to five per $\sqrt{3} \times \sqrt{3}$ unit cell) has been elaborated. DFT analysis revealed that Mg atoms tend to intercalate between the Si substrate and the Tl

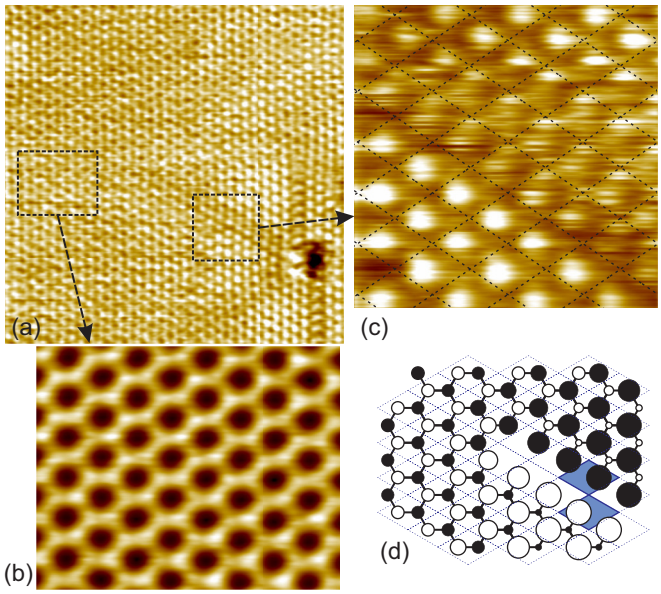


FIG. 2. (a) A 21 × 25 nm$^2$ filled-state STM image of the Si(111) $\sqrt{3} \times \sqrt{3}$ (Tl,Mg) surface. Dashed rectangles mark the honeycomb and hexagonal $\sqrt{3} \times \sqrt{3}$ arrays located far away and close to the structural defect, respectively. High-resolution STM images of the corresponding areas are shown in (b) (averaged 5 × 4 nm$^2$ filled-state STM image) and (c) (5 × 5 nm$^2$ filled-state STM image). (d) Schematic explanation of the formation of two antiphase hexagonal domains from a honeycomb lattice. Black and white circles represent sites of two interpenetrated sublattices and their sizes correspond to the apparent STM height.

layer and any attempt to fix them in the top layer significantly increases the formation energy. The most stable configuration is shown in Fig. 4. The first (bottom) layer includes one Tl atom in the $T_1$ position (referred to as Tl-1 henceforth) caged within a kagomelike lattice of Mg atoms. Both Tl-1 and Mg atoms are practically in the same level (the height difference is only ∼0.01 Å).

The second (top) layer consists only of Tl atoms (four per unit cell) situated on top of the first Tl-Mg layer, breaking its in-plane inversion symmetry. Three of four Tl atoms are located over three Mg atoms, which it looks like a close-packed stacking, and another Tl atom is over the center of the adjacent Mg trimer. This arrangement renders two otherwise equal Mg trimers slightly different; the Mg-Mg bonds labeled *1* and *2* in Fig. 4(d) become 3.26 and 3.44 Å, respectively. Tl-Tl bond lengths in the top layer are 3.32 and 3.38 Å, which are smaller not only compared to the Si(111) 1 × 1 Tl reconstruction (3.84 Å), but also compared to the bulk Tl h.c.p. crystal (3.41 Å [35]).

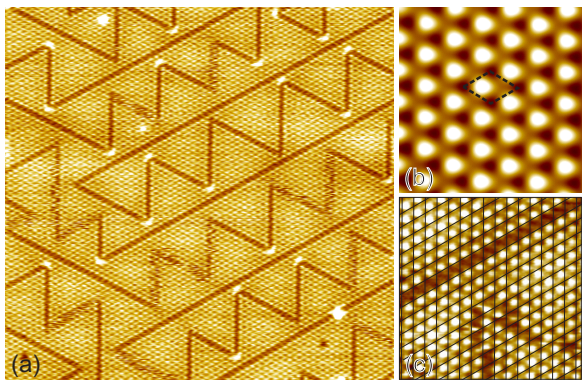


FIG. 3. Low-temperature (110-K) filled-state STM images of the Si(111) $\sqrt{3} \times \sqrt{3}$ TlMg surface: (a) 50 × 48 nm$^2$, (b) 4 × 4 nm$^2$ (averaged), and (c) 10 × 10 nm$^2$ with the $\sqrt{3} \times \sqrt{3}$ lattice superimposed.

The model includes, in total, three Mg atoms (1 ML) and five Tl atoms (1.66 ML). The small deviation of Tl coverage from that obtained experimentally can be attributed to the presence of DWs, which is not considered in the model.

Returning to our STM data we can now describe switching between domains (occurring even at low temperatures) in terms of atomic structure. Figure 4(d) represents an atomic transition between two domains, labeled "I" and "II," separated by the domain wall'. One can see that in this model the bottom layer is almost the same for both domains: Tl-1 atomic positions are the same and Mg atomic positions are shifted by only 0.18 Å, transferring a smaller Mg trimer to another half of the $\sqrt{3} \times \sqrt{3}$ unit cell. The top layer shifts completely so that the Tl trimers in the top layer follow smaller Mg trimers in the bottom layer. On the other hand, Tl atoms at the Si(111) surface are known to be highly mobile [18], so the movement of the top Tl layer seems to be the most probable reason for small changes in the bottom Tl-Mg layer. The STM simulation [Fig. 4(c)] revealed that a bright protrusion observed in experimental STM images is associated with close-packed stacking of Tl and Mg trimers. This structural element shifts from one half of the $\sqrt{3} \times \sqrt{3}$ unit cell to the other after crossing the DW exactly as bright protrusions do in experimental STM images, which confirms the proposed atomic model. At room temperature Tl trimers in the top layer are constantly switching between two Mg trimers in the bottom layer, resulting in an average honeycomb STM appearance with two protrusions per $\sqrt{3} \times \sqrt{3}$ unit cell.

The validity of the model was tested by comparing a calculated band structure with the experimental ARPES spectrum (Fig. 5). It shows a reasonable agreement; all the major bands are reproduced well except for the shape of the band at the $\bar{M}$ point in the $\bar{K}$-$\bar{M}$-$\bar{K}$ direction, which appears more conical in the experiment with a smaller bandgap. Once again we attribute this deviation to the DW presence. (The 1D SBZ associated with the DW coincides with the 2D ($\sqrt{3} \times \sqrt{3}$) SBZ at the $\bar{M}$ points of the latter.)

Details of the Si(111) $\sqrt{3} \times \sqrt{3}$ (Tl,Mg) spin-resolved electronic structure are presented in Fig. 6. There are three major surface-state bands in the bulk bandgap, denoted $S_1$ to $S_3$. Analysis of orbital compositions suggests that top-layer Tl atoms dominate in the formation of these bands, while the bands from Tl-1 and Mg atoms primarily overlap with projected bulk bands as their orbitals are strongly hybridized with the substrate. Furthermore, $S_1$ to $S_3$ bands are mostly generated by $p_x$ and $p_y$ orbitals of the surface atoms [Fig. 6(c)]. The $S_1$ band crosses the Fermi level at a velocity of $1.03 \pm 0.01 \times 10^6$ m/s and displays clear spin-splitting as confirmed by DFT calculations [Fig. 6(b)]. Both $S_2$ and $S_3$ states also have Rashba-type spin-splitting with

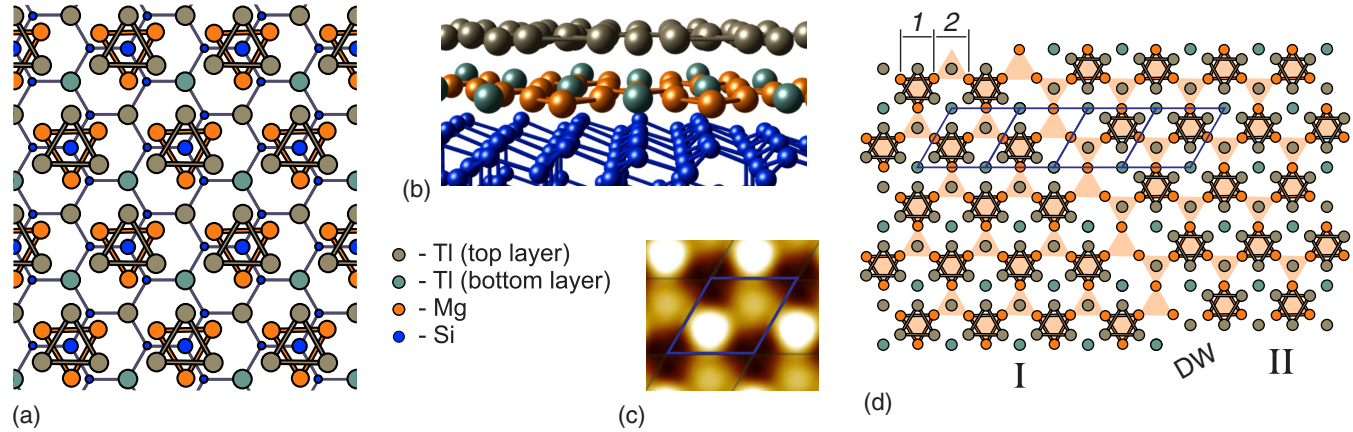


FIG. 4. Atomic structure of the Si(111) $\sqrt{3} \times \sqrt{3}$ (Tl,Mg) surface. (a) Top view and (b) perspective 3D drawing of the ball-and-stick model. Only the shortest Tl-Tl and Mg-Mg bonds are shown, to simplify the image. (c) Simulated STM image. (d) Two possible top-layer stackings (I and II) with respect to the bottom layer. Mg trimers are represented by pink triangles to emphasize the Mg kagome lattice. Numbers *1* and *2* are Mg-Mg bond lengths within and between Mg trimers, respectively.

spin degeneracy at the $\bar{M}$ point, which is consistent with the $C_3$ point group symmetry [36,37]. Note that the $S_3$ band is insulating, with a maximum at the $\bar{M}$ point, while the $S_2$ band has a saddle point there, producing a small divergence in the LDOS [Fig. 6(a)] in the vicinity of the Fermi level (van Hove singularity).

Another interesting characteristic is the presence of two spin-polarized nearly flat bands above $E_F$ around the $\bar{\Gamma}$ point occupying a significant part of the SBZ and thus producing LDOS divergences as well. Typically, flat bands are expected for an ideal kagome lattice from the viewpoint of the nearest-neighbor hopping model [38, and references therein], as well as for a breathing kagome lattice (i.e., with nonequivalent triangles, as in the present case) [39]. It was observed in many experimentally accessible systems, for instance, in the layered kagome metal FeSn [40] and twisted bilayer graphene [41–43]. In the present case, however, the orbital analysis revealed that the flat bands originate not from the breathing kagome lattice of Mg atoms as one would expect, but from $p_z$ orbitals in the top Tl layer [Fig. 6(b)].

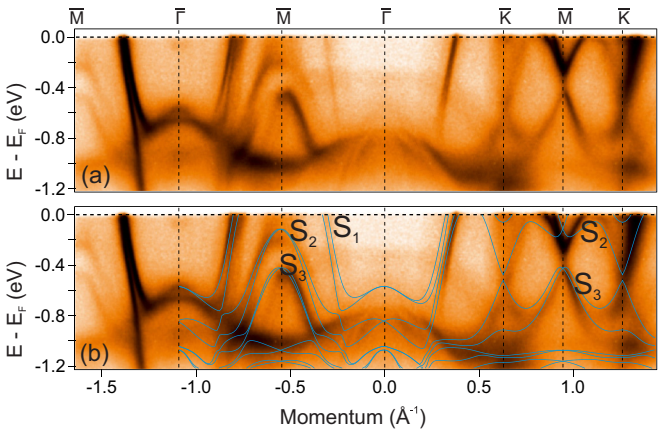


FIG. 5. (a) ARPES spectrum of the $\sqrt{3} \times \sqrt{3}$ (Tl,Mg)/Si(111) surface recorded at 78 K. (b) The same as (a), with the calculated band structure (spin-orbit interaction included) superimposed. The calculated spectrum was shifted by ~0.1 eV towards a higher binding energy to match the experimental spectrum.

The most prominent feature of the (Tl,Mg)/Si(111) band structure is a giant Zeeman-like spin splitting at the $\bar{K}$ point. The cones in $\bar{K}$ points are diverged from Rashba-type spin-split $S_2$ and $S_3$ bands [compare the spectra calculated with and without SOC, in Figs. 6(b) and 6(c), respectively] and show no spin degeneracy at the $\bar{K}$ point. Similarly to reported $1 \times 1$ Tl/Si(111) [13,17,44,45], graphene/Sn/SiC(0001) [46], group VI dichalcogenides [47], and many other systems, spins of both bands point in the direction perpendicular to the surface at $\bar{K}$ and all the in-plain spin components vanish [Figs. 6(d) and 6(e)], which is a general property of this reciprocal lattice point [13]. In contrast to most such systems, the Zeeman-type splitting here is enormous, amounting to 409 and 386 meV for $S_2$ and $S_3$ bands, respectively. In both calculated and experimental spectra cones exhibit a gap directly at the $\bar{K}$ point, which is due to the lack of any mirror symmetries at that point [48].

Note that bands at two $\bar{K}$ points with opposite valley pseudospins, $\bar{K}$ and $\bar{K}'$, have opposite signs of out-of-plain components [Figs. 6(d) and 6(e)] due to the Berry-phase effect on charge carriers. This feature is considered essential for coupling between spin and valley pseudospin and utilizing this new degree of freedom for potential valleytronic devices [17,49,50].

Away from $\bar{K}$ points the in-plane spin components increase. Figure 6(e) shows the experimental Fermi-contour map together with the calculated energy cut superimposed. Around a $\bar{K}$ point one can see a small triangular pocket ($S_2'$ band) and a $\bar{K}$-centered trimer of pockets ($S_2''$) enclosed in a deformed hexagon. Trimers are hardly visible on the experimental map due to the drastic loss in photoemission intensity of the corresponding band ($S_2$ in the $\bar{K} \rightarrow \bar{\Gamma}$ direction; Fig. 5). Another feature is two concentric contours in the shape of a smoothed hexagon with opposite spin polarizations around $\bar{\Gamma}$ points. Around the $\bar{\Gamma}_0$ point its intensity is negligible but it can be clearly spotted around the $\bar{\Gamma}_1$ point, which could be

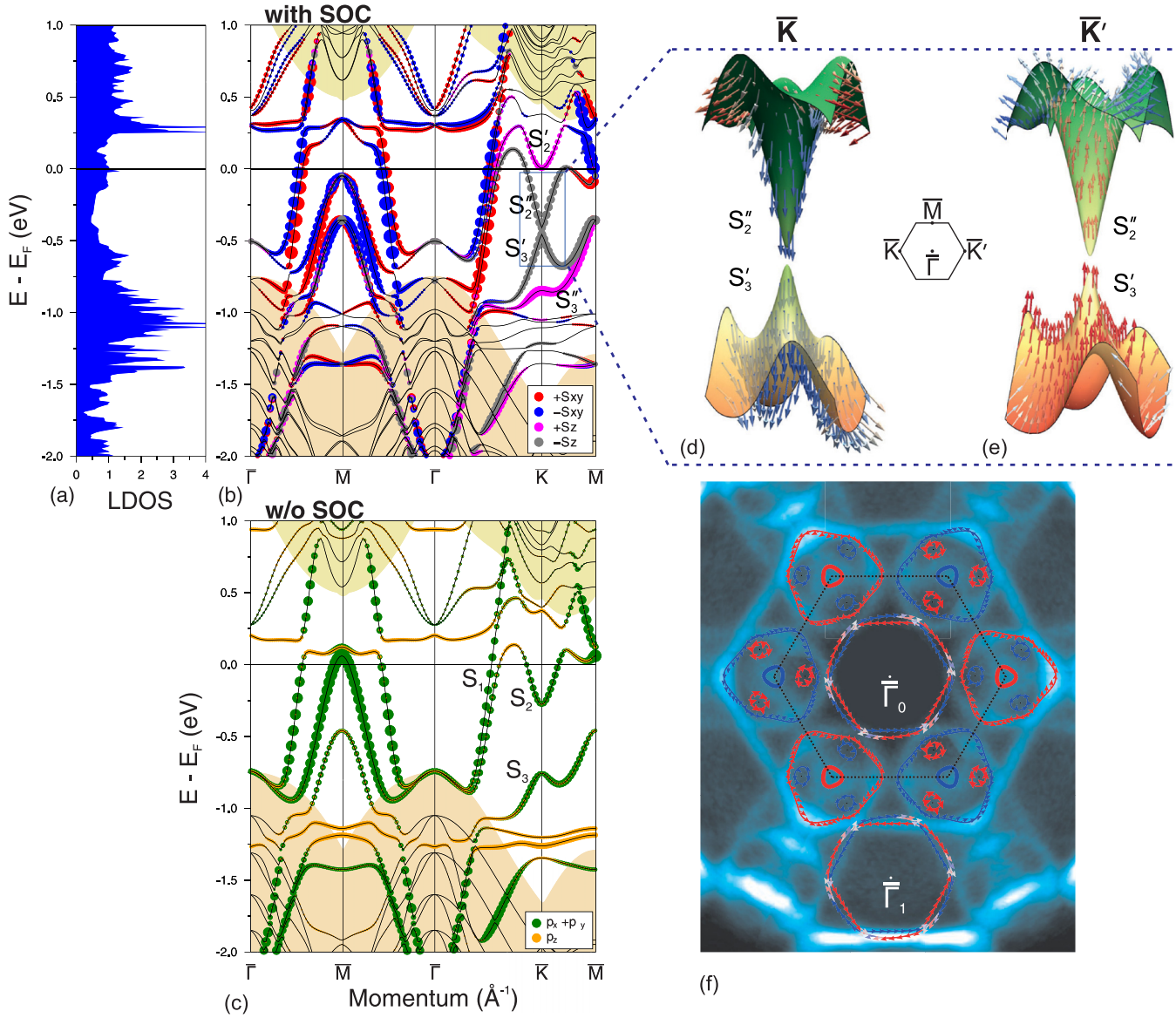


FIG. 6. Electronic properties of the Si(111) $\sqrt{3} \times \sqrt{3}$ (Tl,Mg) surface. (a) Local density of states (SOC is included). (b) Spin-resolved band structure including SOC, indicating in-plain and out-of-plane spin polarization. The red and blue and the magenta and gray circles correspond to the positive and negative $S_{xy}$ and $S_z$ spin components, respectively; the size of the circles indicates the degree of spin polarization. (c) Orbital-resolved band structure without SOC showing orbital contributions of surface atoms. Green and yellow circles correspond to $p_{x,y}$ and $p_z$ orbitals at a particular $k_\parallel$ value, respectively; their size reflects the strength of the surface states. The shaded regions in (a) and (b) indicate projected bulk bands. (d, e) Volumetric zoom-in view of two conical bands at two different $\bar{K}$ points and the associated spin texture. (f) Calculated constant-energy cut superimposed on the experimental Fermi-contour map. The black hexagon marks the $\sqrt{3} \times \sqrt{3}$ unit cell.

explained by the photoemission structure factor effect (see, e.g., [51]).

## IV. CONCLUSIONS

A new double-layer structure is found to form on a Si(111) surface by room-temperature 1-ML Mg deposition onto a Tl-covered surface with total Tl coverage of ∼1.6 ML. Mg atoms substitute for Tl atoms, incorporating between the Tl layer and the Si(111) substrate and forming a breathing kagome lattice with one Tl atom occupying a hexagonal-ring site in it. The rest of the Tl atoms form a second layer with two possible types of stacking, both of which break the inversion symmetry of the structure. At room temperature, Tl atoms in the top layer continuously change their positions in a collective manner, creating the illusion of a honeycomb lattice. The electronic band structure of the (Tl,Mg)/Si(111) 2D compound displays spin-split metallic bands, an almost dispersionless, nearly flat band ∼0.2 eV above and a saddle point ∼0.2 eV below the Fermi level, with corresponding divergences in the LDOS spectra (van Hove singularities). As such, the surface may demonstrate properties associated with a strong correlation of electrons after slight tuning of the Fermi level position. At $\bar{K}$ and $\bar{K}'$ points with opposite valley pseudospins, the bands form gapped cones with opposite out-of-plane spin polarizations.

## ACKNOWLEDGMENTS

The work was supported by the Russian Foundation for Basic Research under Grant No. 18-52-52012 MHT_a, the Ministry of Science and Technology (MOST) of Taiwan (TW) under Grant No. 107-2923-M-001-004-MY3, and the Russian President's Grant No. MK-1341.2020.2 for young researchers. The calculations were conducted using the equipment of the Shared Resource Center "Far Eastern Computing Resource" IACP FEB RAS [52].



[1] T. Zhang, P. Cheng, W.-J. Li, Y.-J. Sun, G. Wang, X.-G. Zhu, K. He, L. Wang, X. Ma, X. Chen, Y. Wang, Y. Liu, H.-Q. Lin, J.-F. Jia, and Q.-K. Xue, Superconductivity in one-atomic-layer metal films grown on Si(111), Nat. Phys. **6**, 104 (2010).

[2] W. Qin, L. Li, and Z. Zhang, Chiral topological superconductivity arising from the interplay of geometric phase and electron correlation, Nat. Phys. **15**, 796 (2019).

[3] Y. Saito, T. Nojima, and Y. Iwasa, Highly crystalline 2D superconductors, Nat. Rev. Mater. **2**, 16094 (2017).

[4] C. Brun, T. Cren, and D. Roditchev, Review of 2D superconductivity: The ultimate case of epitaxial monolayers, Supercond. Sci. Technol. **30**, 013003 (2017).

[5] K. Yaji, Y. Ohtsubo, S. Hatta, H. Okuyama, K. Miyamoto, T. Okuda, A. Kimura, H. Namatame, M. Taniguchi, and T. Aruga, Large Rashba spin splitting of a metallic surface-state band on a semiconductor surface., Nat. Commun. **1**, 17 (2010).

[6] K. Sakamoto, H. Kakuta, K. Sugawara, K. Miyamoto, A. Kimura, T. Kuzumaki, N. Ueno, E. Annese, J. Fujii, A. Kodama, T. Shishidou, H. Namatame, M. Taniguchi, T. Sato, T. Takahashi, and T. Oguchi, Peculiar Rashba Splitting Originating from the Two-Dimensional Symmetry of the Surface, Phys. Rev. Lett. **103**, 156801 (2009).

[7] X.-G. Zhu, Z. Liu, W. Li, J. Wen, X. Chen, J.-F. Jia, X.-C. Ma, K. He, L.-L. Wang, and Q.-K. Xue, Observation of Rashba splitting on reconstructed surface, Surf. Sci. **618**, 115 (2013).

[8] P. Höpfner, J. Schäfer, A. Fleszar, S. Meyer, C. Blumenstein, T. Schramm, M. Heßmann, X. Cui, L. Patthey, W. Hanke, and R. Claessen, Electronic band structure of the two-dimensional metallic electron system Au/Ge(111), Phys. Rev. B **83**, 235435 (2011).

[9] K. Nakatsuji, R. Niikura, Y. Shibata, M. Yamada, T. Iimori, F. Komori, Y. Oda, and A. Ishii, Anisotropic splitting and spin polarization of metallic bands due to spin-orbit interaction at the Ge(111)($\sqrt{3} \times \sqrt{3}$)R30°-Au surface, Phys. Rev. B **84**, 035436 (2011).

[10] P. Höpfner, J. Schäfer, A. Fleszar, J. H. Dil, B. Slomski, F. Meier, C. Loho, C. Blumenstein, L. Patthey, W. Hanke, and R. Claessen, Three-Dimensional Spin Rotations at the Fermi Surface of a Strongly Spin-Orbit Coupled Surface System, Phys. Rev. Lett. **108**, 186801 (2012).

[11] C.-H. Hsu, Z.-Q. Huang, C.-Y. Lin, G. M. Macam, Y.-Z. Huang, D.-S. Lin, T. C. Chiang, H. Lin, F.-C. Chuang, and L. Huang, Growth of a predicted two-dimensional topological insulator based on InBi-Si(111)-$\sqrt{7} \times \sqrt{7}$, Phys. Rev. B **98**, 121404(R) (2018).

[12] D. V. Gruznev, S. V. Eremeev, L. V. Bondarenko, A. Y. Tupchaya, A. A. Yakovlev, A. N. Mihalyuk, J.-p. Chou, A. V. Zotov, and A. A. Saranin, Two-dimensional In–Sb compound on silicon as a quantum spin Hall insulator, Nano Lett. **18**, 4338 (2018).

[13] K. Sakamoto, T. Oda, A. Kimura, K. Miyamoto, M. Tsujikawa, A. Imai, N. Ueno, H. Namatame, M. Taniguchi, P. E. J. Eriksson, and R. I. G. Uhrberg, Abrupt Rotation of the Rashba Spin to the Direction Perpendicular to the Surface, Phys. Rev. Lett. **102**, 096805 (2009).

[14] T. Aruga, Different types of Rashba spin-split surface states on Ge(111), J. Electron Spectrosc. Relat. Phenom. **201**, 74 (2015).

[15] Y. Ohtsubo, S. Hatta, H. Okuyama, and T. Aruga, A metallic surface state with uniaxial spin polarization on Tl/Ge(111)-(1 × 1), J. Phys.: Condens. Matter **24**, 092001 (2012).

[16] J. Ibañez-Azpiroz, A. Eiguren, and A. Bergara, Relativistic effects and fully spin-polarized Fermi surface at the Tl/Si(111) surface, Phys. Rev. B **84**, 125435 (2011).

[17] K. Sakamoto, T.-H. Kim, T. Kuzumaki, B. Müller, Y. Yamamoto, M. Ohtaka, J. R. Osiecki, K. Miyamoto, Y. Takeichi, A. Harasawa, S. D. Stolwijk, A. B. Schmidt, J. Fujii, R. I. G. Uhrberg, M. Donath, H. W. Yeom, and T. Oda, Valley spin polarization by using the extraordinary Rashba effect on silicon, Nat. Commun. **4**, 2073 (2013).

[18] L. Vitali, M. Ramsey, and F. Netzer, Rotational epitaxy of a 'soft' metal overlayer on Si(111), Surf. Sci. **452**, L281 (2000).

[19] A. N. Mihalyuk, L. V. Bondarenko, A. Y. Tupchaya, D. V. Gruznev, J.-P. Chou, C.-R. Hsing, C.-M. Wei, A. V. Zotov, and A. A. Saranin, Double-atomic layer of Tl on Si(111): Atomic arrangement and electronic properties, Surf. Sci. **668**, 17 (2018).

[20] S. Ichinokura, L. V. Bondarenko, A. Y. Tupchaya, D. V. Gruznev, A. V. Zotov, A. A. Saranin, and S. Hasegawa, Superconductivity in thallium double atomic layer and transition into an insulating phase intermediated by a quantum metal state, 2D Mater. **4**, 025020 (2017).

[21] E. Annese, T. Kuzumaki, B. Müller, Y. Yamamoto, H. Nakano, H. Kato, A. Araki, M. Ohtaka, T. Aoki, H. Ishikawa, T. Hayashida, J. R. Osiecki, K. Miyamoto, Y. Takeichi, A. Harasawa, K. Yaji, T. Shirasawa, K.-i. Nittoh, W. Yang, K. Miki, T. Oda, H. W. Yeom, and K. Sakamoto, Nonvortical Rashba Spin Structure on a Surface with $C_{1h}$ Symmetry, Phys. Rev. Lett. **117**, 016803 (2016).

[22] A. V. Matetskiy, S. Ichinokura, L. V. Bondarenko, A. Y. Tupchaya, D. V. Gruznev, A. V. Zotov, A. A. Saranin, R. Hobara, A. Takayama, and S. Hasegawa, Two-Dimensional Superconductor with a Giant Rashba Effect: One-Atom-Layer Tl-Pb Compound on Si(111), Phys. Rev. Lett. **115**, 147003 (2015).

[23] T. Nakamura, A. Takayama, R. Hobara, D. Gruznev, A. Zotov, A. Saranin, and S. Hasegawa, Superconducting single-atomic-layer Tl-Pb compounds on Ge(111) and Si(111) surfaces, Appl. Surf. Sci. **479**, 679 (2019).

[24] D. V. Gruznev, L. V. Bondarenko, A. V. Matetskiy, A. Y. Tupchaya, A. A. Alekseev, C. R. Hsing, C. M. Wei, S. V. Eremeev, A. V. Zotov, and A. A. Saranin, Electronic band structure of a Tl/Sn atomic sandwich on Si(111), Phys. Rev. B **91**, 035421 (2015).

[25] A. V. Matetskiy, N. V. Denisov, A. V. Zotov, and A. A. Saranin, Weak antilocalization at the atomic-scale limit of metal film thickness, Nano Lett. **19**, 570 (2019).

[26] X. Lin, W. Yang, K. L. Wang, and W. Zhao, Two-dimensional spintronics for low-power electronics, Nature Electron. **2**, 274 (2019).

[27] G. Kresse and J. Hafner, Ab initio molecular dynamics for liquid metals, Phys. Rev. B **47**, 558 (1993).

[28] G. Kresse and D. Joubert, From ultrasoft pseudopotentials to the projector augmented-wave method, Phys. Rev. B **59**, 1758 (1999).

[29] P. E. Blöchl, Projector augmented-wave method, Phys. Rev. B **50**, 17953 (1994).

[30] J. P. Perdew, K. Burke, and M. Ernzerhof, Generalized Gradient Approximation Made Simple, Phys. Rev. Lett. **77**, 3865 (1996).

[31] L. G. Ferreira, M. Marques, and L. K. Teles, Approximation to density functional theory for the calculation of band gaps of semiconductors, Phys. Rev. B **78**, 125116 (2008).

[32] L. G. Ferreira, M. Marques, and L. K. Teles, Slater half-occupation technique revisited: The LDA-1/2 and GGA-1/2 approaches for atomic ionization energies and band gaps in semiconductors, AIP Adv. **1**, 032119 (2011).

[33] T. Noda, S. Mizuno, J. Chung, and H. Tochihara, T4 site adsorption of Tl atoms in a Si(111)-(1 × 1)-Tl structure, determined by low-energy electron diffraction analysis, Jpn. J. Appl. Phys. **42**, L319 (2003).

[34] The single-layer (Tl,Mg)/Si(111) structure is beyond the scope of this paper .

[35] C. Lynch, *Handbook of Materials Science: Vol. 1. General Properties* (Routledge Revivals) (CRC Press, Boca Raton, FL, 2019).

[36] M. Nagano, A. Kodama, T. Shishidou, and T. Oguchi, A first-principles study on the Rashba effect in surface systems, J. Phys.: Condens. Matter **21**, 064239 (2009).

[37] T. Oguchi and T. Shishidou, The surface Rashba effect: A $k \cdot p$ perturbation approach, J. Phys.: Condens. Matter **21**, 092001 (2009).

[38] Z. Liu, F. Liu, and Y.-S. Wu, Exotic electronic states in the world of flat bands: From theory to material, Chin. Phys. B **23**, 077308 (2014).

[39] K. Essafi, L. D. C. Jaubert, and M. Udagawa, Flat bands and Dirac cones in breathing lattices, J. Phys.: Condens. Matter **29**, 315802 (2017).

[40] M. Kang, L. Ye, S. Fang, J.-S. You, A. Levitan, M. Han, J. I. Facio, C. Jozwiak, A. Bostwick, E. Rotenberg, M. K. Chan, R. D. McDonald, D. Graf, K. Kaznatcheev, E. Vescovo, D. C. Bell, E. Kaxiras, J. van den Brink, M. Richter, M. Prasad Ghimire, J. G. Checkelsky, and R. Comin, Dirac fermions and flat bands in the ideal kagome metal FeSn, Nat. Mater. **19**, 163 (2020).

[41] E. Suárez Morell, J. D. Correa, P. Vargas, M. Pacheco, and Z. Barticevic, Flat bands in slightly twisted bilayer graphene: Tight-binding calculations, Phys. Rev. B **82**, 121407(R) (2010).

[42] G. Trambly de Laissardière, D. Mayou, and L. Magaud, Localization of Dirac electrons in rotated graphene bilayers, Nano Lett. **10**, 804 (2010).

[43] F. Crasto de Lima, R. H. Miwa, and E. Suárez Morell, Double flat bands in kagome twisted bilayers, Phys. Rev. B **100**, 155421 (2019).

[44] M.-H. Liu and C.-R. Chang, Upstanding Rashba spin in honeycomb lattices: Electrically reversible surface spin polarization, Phys. Rev. B **80**, 241304(R) (2009).

[45] K. Sakamoto, T. Oda, A. Kimura, Y. Takeichi, J. Fujii, R. Uhrberg, M. Donath, and H. W. Yeom, Symmetry induced peculiar Rashba effect on thallium adsorbed Si(111) surfaces, J. Electron Spectrosc. Relat. Phenom. **201**, 88 (2015).

[46] K. Yaji, A. Visikovskiy, T. Iimori, K. Kuroda, S. Hayashi, T. Kajiwara, S. Tanaka, F. Komori, and S. Shin, Coexistence of Two Types of Spin Splitting Originating from Different Symmetries, Phys. Rev. Lett. **122**, 126403 (2019).

[47] D. Xiao, G.-B. Liu, W. Feng, X. Xu, and W. Yao, Coupled Spin and Valley Physics in Monolayers of MoS2 and other Group-VI Dichalcogenides, Phys. Rev. Lett. **108**, 196802 (2012).

[48] G. Vasseur, Y. Fagot-Revurat, B. Kierren, M. Sicot, and D. Malterre, Effect of symmetry breaking on electronic band structure: Gap opening at the high symmetry points, Symmetry **5**, 344 (2013).

[49] X. Xu, W. Yao, D. Xiao, and T. F. Heinz, Spin and pseudospins in layered transition metal dichalcogenides, Nat. Phys. **10**, 343 (2014).

[50] J. R. Schaibley, H. Yu, G. Clark, P. Rivera, J. S. Ross, K. L. Seyler, W. Yao, and X. Xu, Valleytronics in 2D materials, Nat. Rev. Mater. **1**, 16055 (2016).

[51] T. Hirahara, I. Matsuda, and S. Hasegawa, Photoemission structure factor effect for Fermi rings of the Si(111)$\sqrt{3} \times \sqrt{3}$-Ag surface, e-J. Surf. Sci. Nanotechnol. **2**, 141 (2004).

[52] https://cc.dvo.ru